JOURNAL OF GEOPHYSICAL RESEARCH, VOL. 105, NO. A8, PAGES 18,835–18,846, AUGUST 1, 2000

Geomagnetic negative sudden impulse due to a magnetic cloud observed on May 13, 1995

T. Takeuchi,[1] T. Araki,[1] H. Luehr,[2] O. Rasmussen,[3] J. Watermann,[3]
D. K. Milling,[4] I. R. Mann,[4] K. Yumoto,[5] K. Shiokawa,[6] and T. Nagai[7]

Abstract. A geomagnetic negative sudden impulse (SI^-) observed on May 13, 1995, was examined using magnetic field data from ETS VI and GOES 7 in the magnetosphere and ground geomagnetic observation networks. The SI^- was caused by a sudden decrease in the solar wind dynamic pressure at the front boundary of a magnetic cloud embedded in a density enhancement region. The amplitude and the fall time at Kakioka geomagnetic observatory (magnetic latitude 26.9°, magnetic longitude 208.3°) were 26 nT and 10 min, respectively. Although SI^- has been considered to be the mirror image of geomagnetic positive sudden impulse (SI^+) or sudden commencement (SC), we found the polarization distribution of the SI^- consistent with that of SC. We suggest that the contribution from the longitudinal movement of a twin-vortex ionospheric current system is dominant to produce the polarization of SC and SI^-. We also discuss the relationship between the angle at which discontinuities in the solar wind impinge upon the magnetosphere and the geomagnetic response.

1. Introduction

The geomagnetic sudden commencement (SC) or positive sudden impulse (SI^+) begins when the magnetopause is compressed by a sudden enhancement of the solar wind dynamic pressure. The global simultaneous occurrence with clear onsets and well-identified sources are the main characteristics of SC. SCs are favorable phenomena to study the transient response of the magnetosphere, ionosphere, and conducting Earth system to variations of the solar wind dynamic pressure. The SC is not a simple increase in the H component of the geomagnetic field. The model that explains how a simple step function-like increase in the solar wind dynamic pressure causes a complex global distribution of the amplitude and waveform of SC on the ground is well established [see *Araki*, 1977, 1994]. *Wilson and Sugiura* [1961] reported that the horizontal vector of SC observed at high-latitude was circularly polarized and concluded that it indicated hydromagnetic waves in the magnetosphere. They proposed a polarization rule that the sense of the polarization is counterclockwise in the morning and clockwise in the afternoon. Using data from the North American International Magnetospheric Study (IMS) Magnetometer Network, which include stations in the polar cap, *Araki and Allen* [1982] demonstrated a latitudinal reversal of the sense of the polarization of SC around 64°-72° latitude.

The geomagnetic response to a sudden expansion of the magnetosphere is called negative sudden impulse (SI^-). Although SCs have been examined by many investigators, detailed analysis of SI^-s has not been made except for *Araki and Nagano* [1988]. They studied five successive SI^-s and confirmed that geomagnetic variations of the SI^- observed in the magnetosphere and on the ground were well explained by the SC model by reversing the direction of the electric current used in the model. Whether or not the sense of SI^- polarization obeys the polarization rule of *Wilson and Sugiura* [1961] was not demonstrated in their study because of the lack of high time resolution geomagnetic data. This is one of reasons why we have made a comprehensive study of an SI^- in this paper.

The SI^- we analyzed here occurred at around 1200 UT on May 13, 1995. *Takeuchi et al.* [1998] examined a sudden expansion and deformation of the Earth's bow shock associated with the SI^-. They reported that the sudden drop in the dynamic pressure was due to a tangential discontinuity, which was the front boundary of a

[1]Department of Earth and Planetary Science, Kyoto University, Kyoto, Japan.
[2]GeoForschungs Zentrum, Potsdam, Germany.
[3]Danish Meteorological Institute, Copenhagen.
[4]Department of Physics, University of York, York, England.
[5]Department of Earth and Planetary Sciences, Kyushu University, Fukuoka, Japan.
[6]Solar-Terrestrial Environment Laboratory, Nagoya University, Japan.
[7]Department of Earth and Planetary Sciences, Tokyo Institute of Technology, Japan.

Paper number 2000JA900055.
0148-0227/00/2000JA900055$09.00

magnetic cloud embedded in a density enhancement region. It was also mentioned that the discontinuity-bow shock/magnetosphere interaction started from duskside and southside. We therefore have a clear geometrical image of the structure in the solar wind causing the SI$^-$. This is another motivation for our study because there has been no previous work about the relationship between the geomagnetic response and the geometrical configuration of the solar wind structure.

2. SI$^-$ in the Magnetosphere

2.1. Observations

The top plot in Figure 1a shows a plot of the solar wind dynamic pressure from 1010 to 1050 UT measured by the Wind spacecraft 244 R_E upstream of the Earth. The dynamic pressure decreased from 7.07 nPa at 1023 UT to 0.63 nPa at 1026 UT. The next three plots show corresponding field variations from 1140 to 1220 UT observed in the magnetosphere and at Kakioka (KAK) on the ground. The amplitude and the fall time of the SI$^-$ at KAK (2100 LT) were 26 nT and 10 min, respectively.

The second plot in Figure 1a shows the 3 s magnetic field data obtained by Engineering Test Satellite (ETS) VI [*Nagai et al.*, 1996] located at 38,000 km (5.9 R_E) geocentric distance, 9.6° geographical latitude, and 1630 LT. The base value is calculated from the International Geomagnetic Reference Field (IGRF) 95 geomagnetic main field model. The difference between the ETS VI data and the IGRF 95 is shown, where $B_{||}$ indicates the magnetic field component parallel to the model field. At 1152:45 UT, $B_{||}$ dropped suddenly and then decreased gradually until ~ 1201:21 UT. Around 1205 and 1210 UT, spiky variations were detected, the cause of which is not clear. The fall time was ~ 8.6 min, and the amplitude was ~ 24 nT.

The geostationary satellite GOES 7 was located at 0300 LT in the night sector. The bottom plot in Figure 1a shows the 3.06 s magnetic field data of the H_p component parallel to the rotation axis of the Earth. GOES 7 detected the disturbance ~155 s after ETS VI (the onset time was around 1155:20 UT). It should be noted that the variation of the H_p component was positive with an amplitude of 10 nT. It is not clear whether the total magnetic field strength increased or decreased because the H_e (earthward) and H_n (eastward) components were not measured.

The satellite locations and onset times of the SI$^-$ event are summarized in Figure 1b. Two curves, BS and MP, denote the location of bow shock and magnetopause, respectively, before the SI$^-$, and a dashed circle represents geostationary orbit. The solid lines TD indicate the discontinuity (deformation at the bow shock is not considered) in the solar wind [*Takeuchi et*

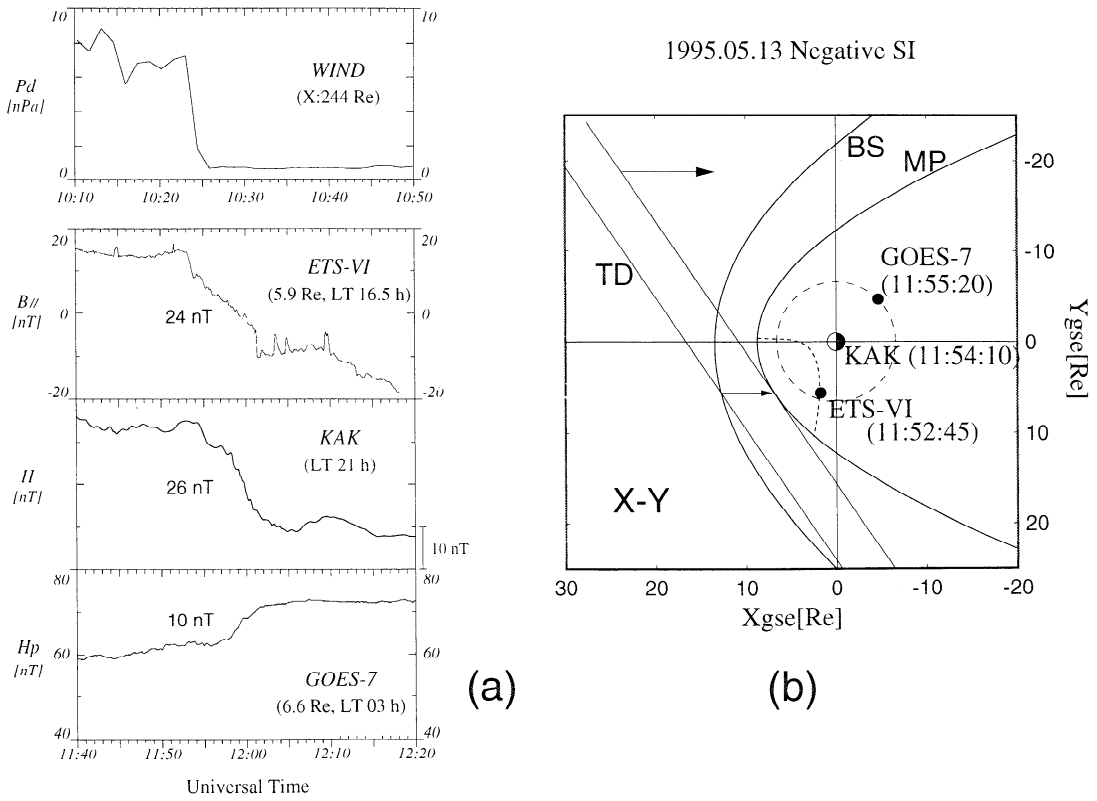

Figure 1. (a) Change in the solar wind dynamic pressure and corresponding SI$^-$ in the magnetosphere and on the Earth observed on May 13, 1995. The amplitude of the variation is given for the magnetic field data. (b) Positions of satellites, magnetopause (MP), and bow shock (BS) before the SI$^-$. The TD indicates the discontinuity in the solar wind.

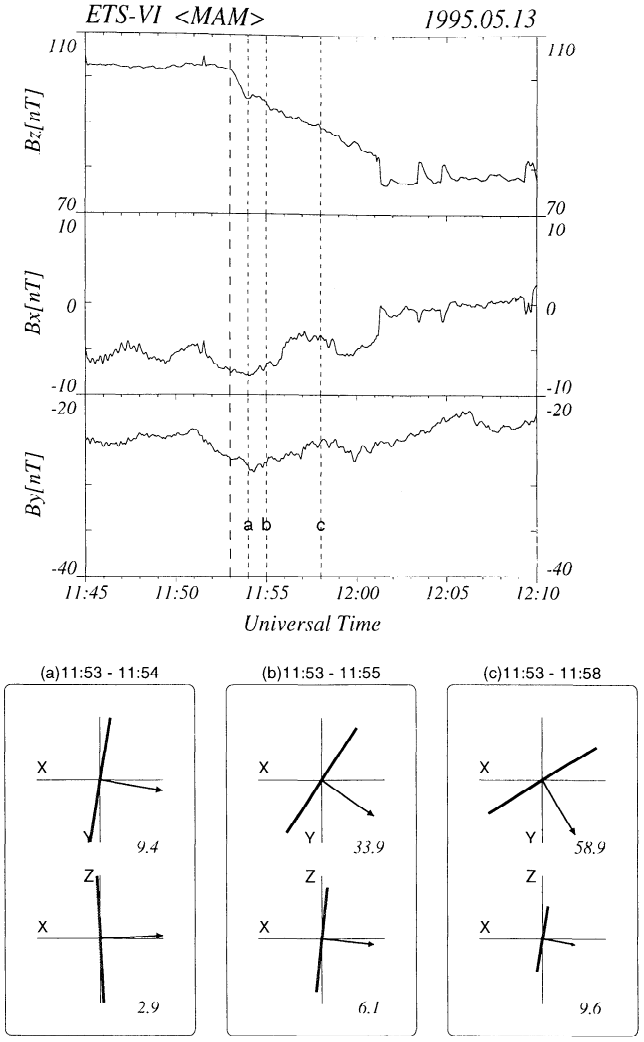

Figure 2. ETS VI magnetic field data in the GSE coordinates and the wave normals obtained by the minimum variance analysis for several intervals from (a) 1153 to 1154 UT, (b) to 1155 UT, and (c) to 1158 UT. Arrows in the bottom plots are the projection of the minimum variance direction to the XY and XZ plane. Numbers represent the angle between the arrows and the X_{GSE} axis.

al., 1998]. The discontinuity was inclined dawnward and should impinge upon the magnetopause in the afternoonside.

2.2. Analysis of the Wavefront in the Magnetosphere

We performed minimum variance analysis to determine the normal direction of the rarefaction wavefront at ETS VI. (Minimum variance analysis for GOES 7 was impossible because of the lack of the azimuthal components of the magnetic field.) Figure 2 shows magnetic field data in the GSE coordinate system. The start time was fixed at 1153 UT, indicated by a long-dashed line. Three end times 1154 UT (labeled a), 1155 UT (labeled b), and 1158 UT (labeled c) were tried, as represented by short-dashed lines. Results of the analysis for each interval are shown in the bottom plot, where arrows indicate the projection of the minimum variance direction to the XY and XZ plane. The direction of the wave normal in the XY plane changes systematically from tailward to duskward with increasing time.

These results can be interpreted as follows. In general, SCs in the magnetosphere propagate across the geomagnetic field lines with phase velocity from 300 to 1000 km/s consistent with known magnetospheric fast mode velocities [*Araki*, 1994]. In the case under consideration, the convection velocity of the discontinuity outside the magnetosphere was $\sim$ 330 km/s [*Takeuchi et al.*, 1998]. The fast mode velocity within the magnetosphere would be higher than the convection velocity of the discontinuity. The leading edge of the disturbance launched at the afternoonside magnetopause would become like the dashed curve shown in Figure 1b and the normal direction pointed tailward at the location of ETS VI. After the discontinuity touched the duskside magnetopause, sources of hydromagnetic waves moved both dawnward and duskward along the magnetopause. The perturbation generated at the dawnside magnetopause should arrive at ETS VI later than that generated at the duskside magnetopause. Therefore the longer the interval we use for the minimum variance analysis, the more the minimum variance direction points duskward. Although affected by the satellite position, the change in the wave normal direction of SI must include information about the angle at which interplanetary shocks or discontinuities impinge upon the magnetosphere.

2.3. SI$^-$ Near Midnight at Geosynchronous Orbit

The northward magnetic field component measured by GOES 7 increased in spite of the expansion of the magnetosphere. *Kokubun* [1983] showed a strong local time dependence of the normalized SC amplitude in H_p at GOES. The normalization was made on the basis of the average amplitude of seven ground stations at low-latitudes. The amplitude became very small (sometimes negative) near midnight. He suggested that the ring current enhancement affected it. *Nagano and Araki* [1986] confirmed a seasonal variation of geosynchronous SC amplitudes near midnight (2100 $\sim$ 0300 LT). SC amplitudes in the geomagnetic H component normalized by the value at Honolulu were smaller in the Northern Hemisphere winter than in the summer. They suggested that the seasonal variation was caused by the change in the position of the tail current sheet relative to the geographic equator. The SI under consideration occurred near the summer solstice. We computed the expected field variation quantitatively using a realistic model of the magnetosphere, Tsyganenko 96 (T96) [see *Tsyganenko and Stern*, 1996]. Input parameters observed were as follows: P_d=7.07(nPa), IMF-(B_y, B_z)=(4.38, 5.69)(nT), and Dst−24 before the SI$^-$ and P_d=0.63(nPa), IMF-(B_y, B_z)=(0.66, 13.44)(nT), and

Dst=-5 after the SI$^-$ [*Takeuchi et al.*, 1998]. An increase of 4.82 nT in the H_p component at GOES 7 was obtained, which is qualitatively consistent with the observation, although the amplitude was slightly smaller. We also concluded from the T96 model that the contribution from the tail current was larger than that from the ring current. Finally, it should be kept in mind that the relative positions of geostationary satellites to the tail current sheet is determined by their longitudes. Therefore the result by *Nagano and Araki* [1986] might be in the opposite sense if the GOES satellites were located elsewhere, for example, at 135° east.

3. Geomagnetic Response

3.1. Background SC Model

Three different physical processes are considered to occur during an SC [see *Araki*, 1977, 1994]. When the magnetosphere is suddenly compressed, a compressional hydromagnetic (HM) wave propagates across the geomagnetic field down to the low- and middle-latitude ionosphere. The wavefront is carried by a dusk-to-dawn polarization current that connects to an enhanced dawn-to-dusk magnetopause current. The HM wave produces a stepwise increase in the geomagnetic H component, the amplitude of which is largest at the equator and decreases with increasing latitude. This field is denoted DL, which means a disturbance dominant in low-latitude regions. Simultaneously, a dusk-to-dawn electric field along the compressional HM wavefront propagating in the dayside magnetosphere is transmitted to the polar ionosphere by a transverse HM wave converted from the compressional mode [*Tamao*, 1964]. This electric field induces twin-vortex ionospheric currents which produce a sharp pulse called preliminary impulse (PI). This field is denoted DP_{pi} (DP means the disturbance field of polar origin). The PI appears as a clear negative impulse of the H component in the afternoonside auroral latitudes and at the dayside equator, which is frequently called a preliminary reverse impulse (PRI). In the morningside auroral latitudes the PI appears as a positive impulse of the H component. The twin-vortex current for the DP_{pi} was first proposed by *Nagata and Abe* [1955] as the equivalent current system, modified by *Araki et al.* [1985], and detected as an actual current by the Magsat satellite [*Araki et al.*, 1984].

After the tailward passage of the compressional wavefront, the magnetospheric convection will be intensified by the enhanced dynamic pressure if it is continuously kept up behind the interplanetary shock. As a result, the dawn-to-dusk convection electric field is enhanced. It is also transmitted along geomagnetic lines of force to the polar ionosphere to produce a twin-vortex ionospheric current system with a sense opposite to that of the DP_{pi} field. This current system produces the main impulse (MI) of polar origin, which is called DP_{mi} field. Thus the disturbance field of an SC is decomposed into three subfields,

$$D_{SC} = DL + DP_{pi} + DP_{mi},$$

each of which has a different dependence on latitude and local time.

3.2. Overview of Geomagnetic Observations

A simple decrease of the H component observed at KAK shown in the third plot of Figure 1a would be mainly due to the DL field. Table 1 provides a list of middle- and high-latitude stations of the geomagnetic

Table 1. Stations of Networks Used in the Analysis

	Geographic		Geomagnetic	
Code	Latitude	Longitude	Latitude	Longitude
	210° Magnetic Meridian (1 s)			
TIK	71.59	128.78	65.67	196.88
CHD	70.62	147.89	64.67	212.12
ZYK	65.75	150.78	59.62	216.72
MGD	59.97	150.86	53.56	218.66
	SAMNET (5 s)			
OUL	65.10	25.85	61.54	105.76
NOR	64.37	13.36	61.45	95.37
NUR	60.51	24.66	56.83	102.53
KVI	59.50	17.63	56.03	96.27
GML	57.16	356.32	54.94	78.15
	IMAGE (10 s)			
NAL	78.92	11.95	76.07	112.25
LYR	78.20	15.82	75.12	113.00
HOR	77.00	15.60	74.02	110.48
HOP	76.51	25.01	72.93	115.91
BJN	74.50	19.20	71.33	108.73
SOR	70.54	22.22	67.24	106.71
KEV	69.76	27.01	66.21	109.73
TRO	69.66	18.94	66.54	103.44
MAS	69.46	23.70	66.07	106.92
KIL	69.02	20.79	65.78	104.31
MUO	68.02	23.53	64.62	105.70
PEL	66.90	24.08	63.46	105.38
OUJ	64.52	27.23	60.89	106.54
HAN	62.30	26.65	58.62	104.99
NUR	60.50	24.65	56.81	102.54
	Greenland Network (20 s)			
THL	77.48	290.83	88.46	14.10
SVS	76.02	294.90	86.79	25.84
KUV	74.57	302.82	84.61	42.26
UPN	72.78	303.85	82.88	37.44
UMQ	70.68	307.87	80.45	39.95
GDH	69.25	306.47	79.27	34.63
ATU	67.93	306.43	78.01	32.61
STF	67.02	309.28	76.83	36.25
SKT	65.42	307.10	75.52	30.94
GHB	64.17	308.27	74.19	31.68
FHB	62.00	310.32	71.86	33.09
NAQ	61.18	314.57	70.59	38.60
MCN	73.93	322.38	80.91	74.02
MCW	72.00	317.41	80.24	59.81
MCE	72.57	326.10	79.18	73.77
AMK	65.60	322.37	73.72	53.95
NRD	81.60	343.33	80.88	131.60
DMH	76.77	341.37	79.20	105.02
DNB	74.30	339.78	77.88	94.29
SCO	70.48	338.03	75.26	82.02

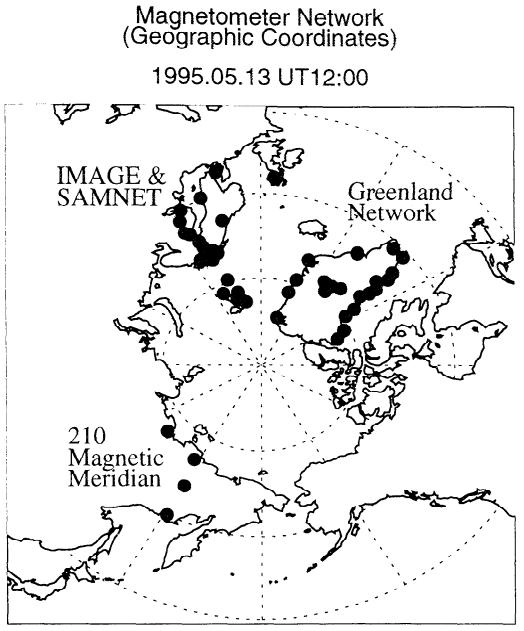

Figure 3. The location of geomagnetic observation networks when the SI⁻ was observed. The direction to the Sun is upward.

networks (210° Magnetic Meridian, Sub-Auroral Magnetometer Network (SAMNET), International Monitor for Auroral Geomagnetic Effects (IMAGE), and Greenland Network) used in the following analysis. The latitude and longitude are given in both geographic and geomagnetic (dipole) coordinate system. The location of the networks at 1200 UT is shown in Figure 3.

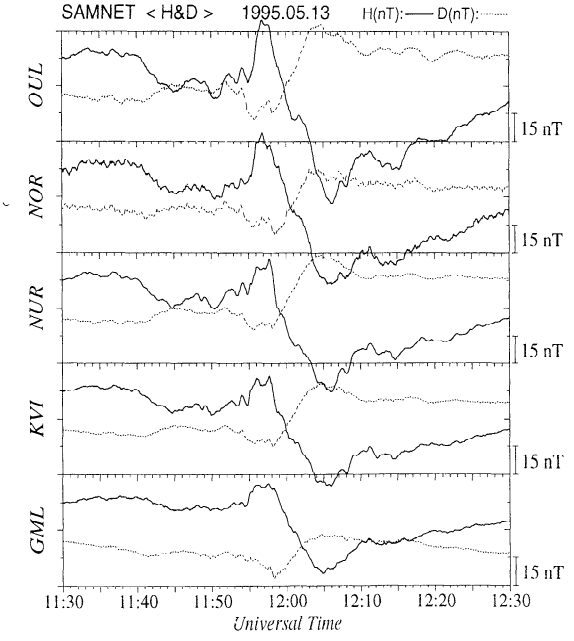

Figure 4. The SI⁻ observed by Sub-Auroral Magnetometer Network (SAMNET) in the afternoon sector (1300-1400 LT). Solid line and dashed line represent the H and D components, respectively. The station code is indicated at the left of each plot.

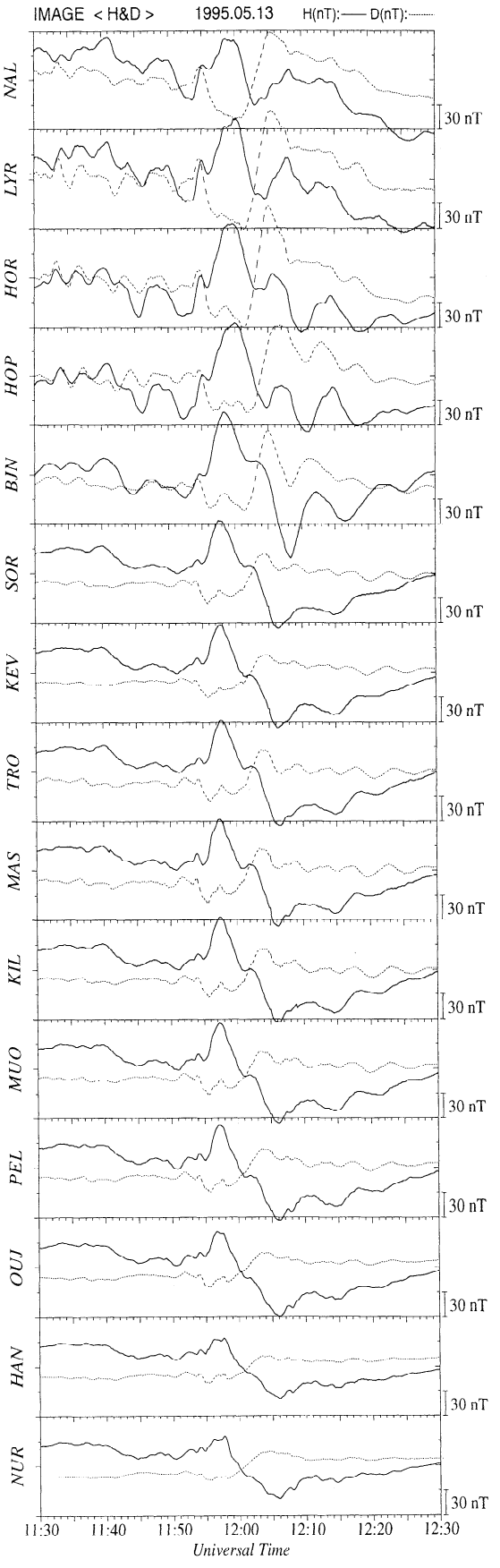

Figure 5. The SI⁻ observed by International Monitor for Auroral Geomagnetic Effects (IMAGE) in the afternoon sector (1300-1400 LT).

3.2.1. SAMNET. Geomagnetic field data (5 s values) from SAMNET are plotted in Figure 4. The solid lines and dashed lines indicate the H and D components, respectively. This observation was made in the afternoon sector (1300-1400 LT). The H component disturbance consists of a positive impulse followed by a negative impulse, which is in the opposite sense to SCs observed at high-latitude stations in the afternoon-side. The D component variation is a negative impulse followed by a positive impulse. The amplitudes of both impulses become larger with increasing latitude.

3.2.2. IMAGE. Figure 5 shows a plot of the variations of the H and D components of the geomagnetic field (10 s values) observed by IMAGE located between 1300 and 1400 LT. The variation is similar to that detected by SAMNET and consists of a positive impulse followed by a negative impulse in the H component and a negative impulse followed by a positive impulse in the D component. Pulsations continuously exist before the SI$^-$ at five higher-latitude stations (NAL, LYR, HOR, HOP, and BJN). Small pulsations can also be seen at lower stations after the first impulse of SI$^-$, which appear clearly in the D component. The period of the pulsations is $\sim$ 4 min. These disturbances are superposed on the SI$^-$ field, and a complicated waveform is produced.

3.2.3. Greenland Network. Stations of Greenland Network are located along the west and east coasts and inland as shown on the map in Figure 6. Figure 6 shows plots of the H and D components of geomagnetic variations (20 s values) observed in Greenland (0800-1100 LT). They are arranged according to the location of the stations. At lower-latitude stations along the west coast a negative impulse in the H component is followed by a positive one. This is opposite to SCs observed in the morning sector. The sense reverses at the higher-

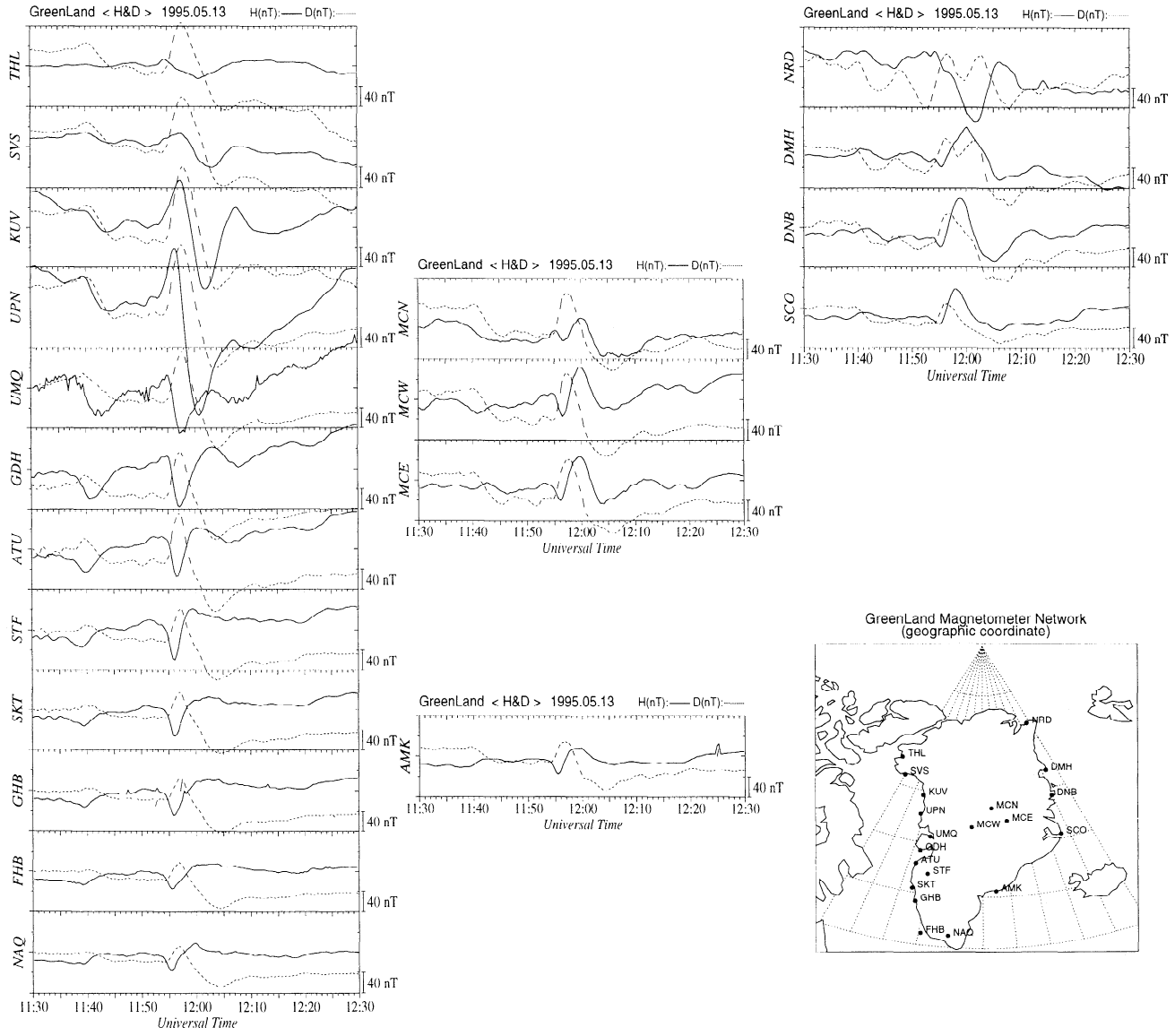

Figure 6. The SI$^-$ observed by Greenland Network in the morning sector (0800-1100 LT). Plots are arranged according to the location of stations.

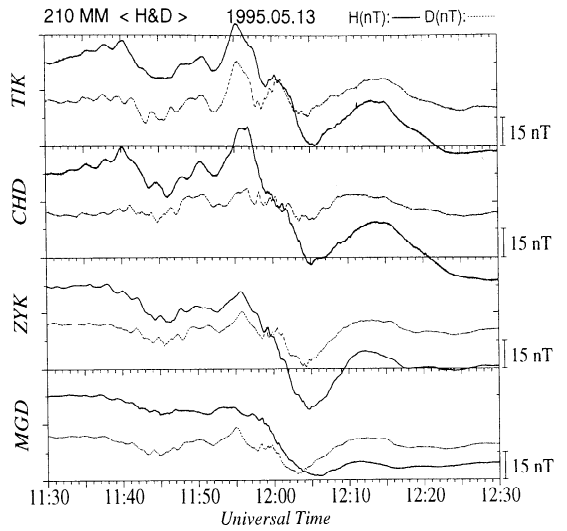

Figure 7. The SI$^-$ observed by 210° Magnetic Meridian Network in the night sector (~2100 LT).

latitude stations (THL, SVS, KUV, and UPN). The transition seems to occur between UPN and UMQ. The amplitude of the H component during the PI reaches a maximum value of ~ 140 nT at UPN (magnetic latitude (MLAT) 82.88°). The impulse around 1156 UT is smaller in amplitude at inland stations and stations on the east coast. The D component variation is a positive impulse followed by a negative impulse at almost all stations.

3.2.4. 210° Magnetic Meridian. Figure 7 shows 1 s sampled geomagnetic data from the stations higher than 50° MLAT along the 210° Magnetic Meridian Chain [*Yumoto et al.*, 1996] in the night sector (~2100 LT). A positive impulse followed by a negative pulse of the H component is observed. Such a waveform disappears at MGD. The D component variation, which is small, is a positive impulse followed by a negative impulse. It is more complicated at TIK.

3.3. Equivalent Current System

Figure 8 shows the equivalent current system for the PI deduced from the ground geomagnetic variations between 1154 and 1157 UT. We used 1 min geomagnetic data from routine observatories archived at the World Data Center for Geomagnetism, Kyoto (not listed in Table 1) as well as data from the geomagnetic networks referred to above. The arrows are drawn with the same length to emphasize the current pattern. A clear twin-vortex current pattern exists during the PI. The rotational sense of the current vortex is clockwise in the morning and counterclockwise in the afternoon, which is opposite to that of SC. The east-west component of the current arrows changes its sign near 82° MLAT around 9 hours MLT and between 76° and 81° MLAT around 16 hours MLT. These are the centers of the current vortices. The demarcation lines between the two vortices lie around 10 hours MLT and 3 hours MLT. The afternoonside current vortex is extraordinarily large. The directions of the twin-vortex equivalent current arrows indicate that a dawn-to-dusk electric field was impressed on the polar ionosphere during the initial phase of the expansion of the magnetosphere. The dawn-to-dusk electric field is considered to be produced along the rarefaction wavefront propagating tailward in the dayside magnetosphere.

3.4. Analysis of the Peak Time of PI

Figure 9 shows a distribution of nominal peak time of the positive PI in the H component versus magnetic latitude (Figure 9a) and PI amplitude (Figure 9b). The Greenland Network stations are not included because the declination angle is very large at Greenland and the variation of the H component cannot simply be compared with other stations. Observations at NAL, LYR, HOR, HOP, and BJN of IMAGE are not used either because pulsations superposed on the SI field affect the nominal peak time of the PI. The circles and squares indicate the observation at the dayside and nightside, respectively. A clear linear relationship exists. As the MLAT or PI amplitude becomes smaller, the nominal PI peak time becomes earlier. This result is interpreted as follows. The disturbance field of SI$^-$ is a superposition of DL (negative) and DP (positive, here) subfields that are dominant at low- and high-latitude, respectively. The MLAT or PI amplitude can be considered as the indicator of the ratio of DP to DL. The nominal peak time of positive PI varies depending on its amplitude relative to the DL field. The smaller (larger) DP becomes or larger (smaller) DL becomes, the ear-

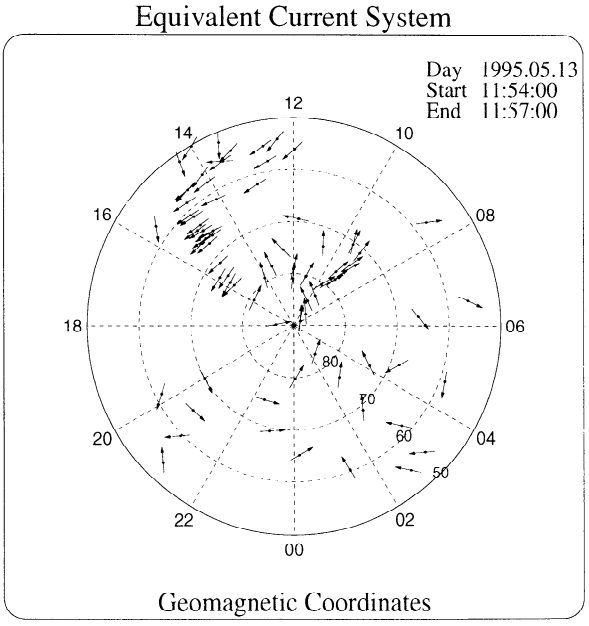

Figure 8. Equivalent current system for the preliminary impulse of the SI$^-$. The arrows are drawn with the same length to emphasize the current pattern.

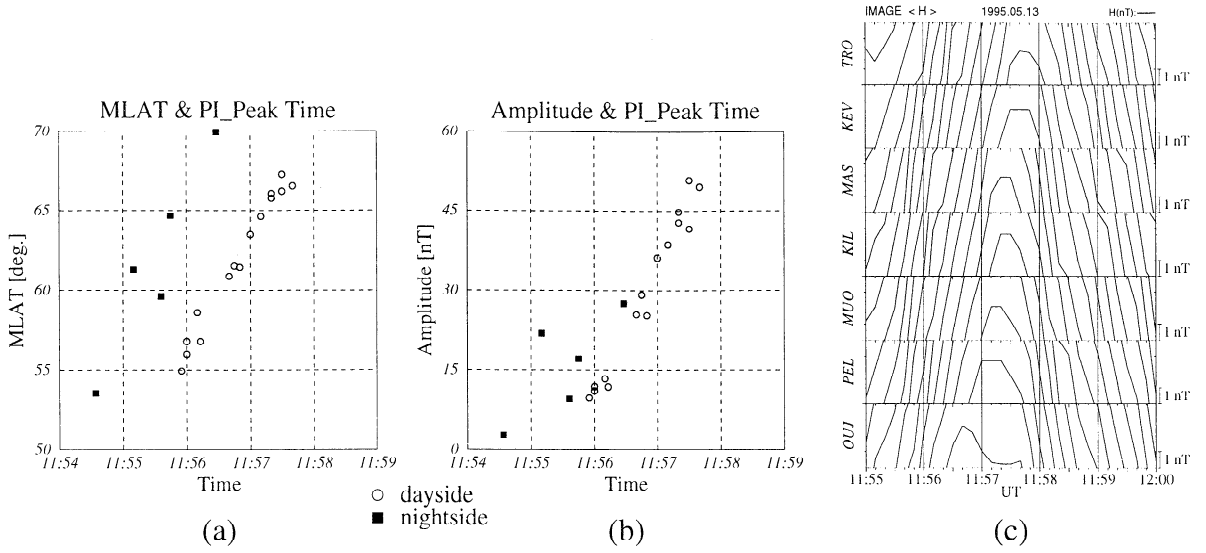

Figure 9. Distribution of the nominal peak time of PI versus (a) MLAT and (b) PI amplitude. Circles and squares indicate the observation in the dayside and nightside, respectively. (c) An example of the shift of PI peak time observed by IMAGE. The data are folded once they exceed the maximum plotting range in the y direction.

lier (later) the nominal peak time of PI becomes. If the contribution of DL was zero, the nominal peak time should be the same as that of a pure DP_{pi}. An example of the shift of PI peak time is shown in Figure 9c observed by IMAGE. The peak time in the night side is earlier than in the dayside even for the same MLAT. The amplitude of the DP field in the night sector must be small as compared with that on the dayside due to the reduced ionospheric conductivity. There is approximately a ~90 s shift of the peak time per 10° MLAT. The linear relation might not be sustained at higher-latitudes because the DL field becomes negligible at magnetic latitudes higher than 70° as can be seen in Figure 6.

3.5. Characteristics of Polarization

Figure 10 shows the polarization distribution of the SI^- during the PI. Each hodogram is drawn for the first 4 min after the onset (1154 UT) when the PI was observed at almost all stations. Observations from some high-latitude observatories provided by WDC for Geomagnetism, Kyoto are also included (LRV, 11.8 hours MLT, MLAT 69.5°; ABK, 14.7 hours MLT, 65.9°; OTT, 6.6 hours MLT, 56.07°; ESK, 12.6 hours MLT, 57.9°; VAL, 12.0 hours MLT, 55.9°). A vertical dashed line indicates local noon. A horizontal dashed line is drawn at 80° MLAT. The following features can be noticed.

1. In the afternoon (A in Figure 10), the rotational sense is roughly clockwise.

2. A counterclockwise rotation followed by clockwise rotation can be seen at NAL, LYR, HOP, and BJN in the afternoon, where the pulsation is superposed on the SI^- field (see Figure 5). The contamination of counterclockwise rotation is largest at LYR.

3. At lower-latitude in the morning (B in Figure 10), the rotational sense is almost counterclockwise, except for OTT in the early morning (0700 LT). Even at stations where pulsations are not observed (Greenland), the magnetic field rotates smoothly.

4. At higher-latitude in the morning (C in Figure 10), the rotational sense is clockwise (UPN and NRD) or linear (UMQ and THL).

5. The latitudinal reversal of the sense of polarization occurs at a magnetic latitude around 80°, which is consistent with the latitude of the foci of the twin-vortex-type equivalent current shown in Figure 8.

6. The amplitude of the disturbance vector takes its maximum value not at the latitude of the polarization reversal but poleward of it.

The properties described in points 1, 3, 4, and 6 are consistent with results of past work on SCs [*Wilson and Sugiura,* 1961; *Araki and Allen,* 1982]. The distribution of polarization sense of SI^- is not opposite to but similar to that of SC. We will further discuss characteristics of the polarization in section 4, including the points 2 and 5.

4. Discussion

It is well known that a damped type magnetic pulsation, called Psc, appears associated with SC [*Saito and Matsushita,* 1967]. The Psc is interpreted as field line resonance whose period depends on latitude and which occurs in a relatively localized region. The sense of polarization of geomagnetic pulsations with a period of several minutes is counterclockwise during night and in the morning (2000-1300 LT) and clockwise in the afternoon (1300-2000 LT) at subauroral latitudes [*Sam-*

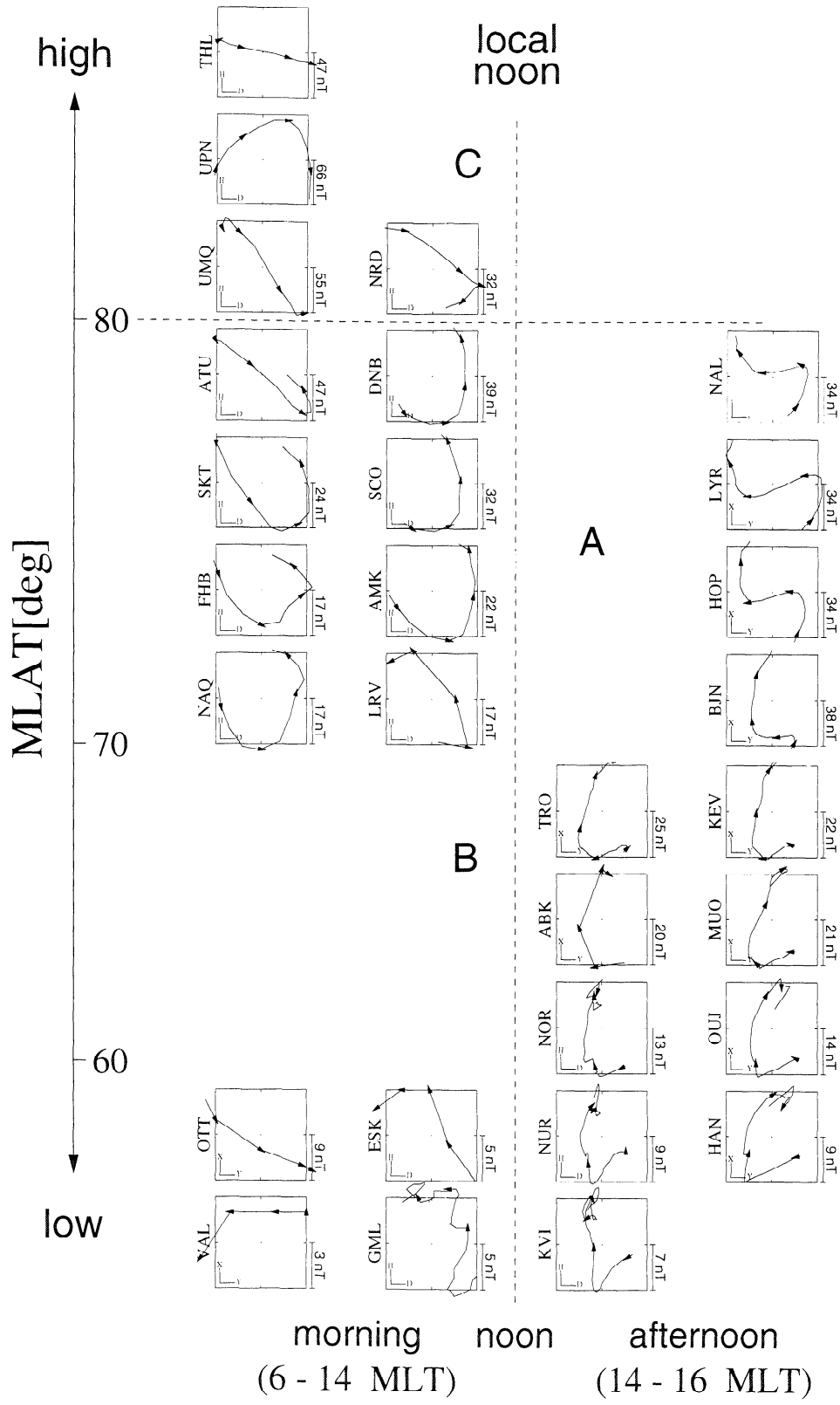

Figure 10. Polarization distribution of the SI^-. The hodograms are drawn for 4 min from 1154 to 1158 UT and are arranged according to the location of the stations. Dashed lines roughly divide the distribution into three parts (A, B, and C) based on the rotational sense of the polarization.

son et al., 1971]. It reverses across a boundary located between 60° and 70° magnetic latitude. The LT dependence is roughly consistent with the SC polarization rule of *Wilson and Sugiura* [1961]. *Araki and Allen* [1982] found a similar latitudinal reversal of polarization for SC.

Figure 5 shows that pulsations are superposed on the PI around 1155 UT with large amplitudes at higher-latitude stations (NAL-BJN). The amplitude seems to be largest at LYR or HOR. A mixed polarization, whose sense of rotation is counterclockwise at first and then clockwise, is seen at the higher-latitude stations of IMAGE (NAL, LYR, HOP, and BJN) in Figure 10. The sense of the polarization is clockwise at the other IMAGE stations. The contamination of counterclockwise rotation is largest at LYR. It is reasonable to consider that this counterclockwise rotation is associated with the pulsation superposed on the PI. A smooth elliptic polarization can be seen even at stations where no pulsations are observed (e.g., stations in Greenland). Therefore we need to consider mechanisms other than pulsations which would rotate the geomagnetic field during PI.

Figure 11 is a schematic picture described by *Nagano et al.* [1985] to explain the SC polarization at geostationary orbit. The magnetospheric compression produces tailward bending of the magnetic field lines of the outer magnetosphere. The rotational sense is clockwise in the morning and counterclockwise in the afternoon when viewed from above the North Pole. When the rotation is projected along lines of force to the polar ionosphere, the rotational sense becomes counterclockwise in the morning and clockwise in the afternoon. This model can explain the polarization distribution both in the magnetosphere and on the ground at the time of SC. When the magnetosphere expands, however, the polarization produced by this model is opposite to that of SC. This model cannot therefore account for the field rotation observed on the ground.

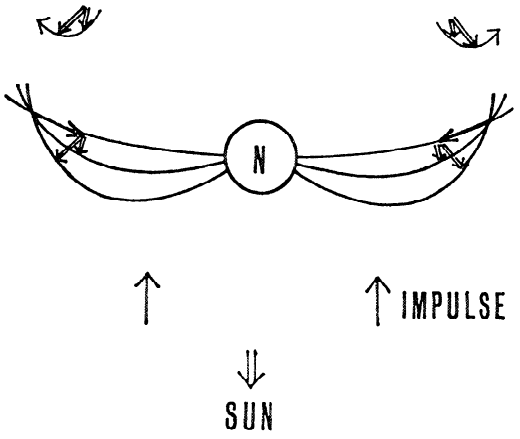

Figure 11. Schematic picture describing the rotational sense of SC vector viewed from above the North Pole [*Nagano et al.*, 1985].

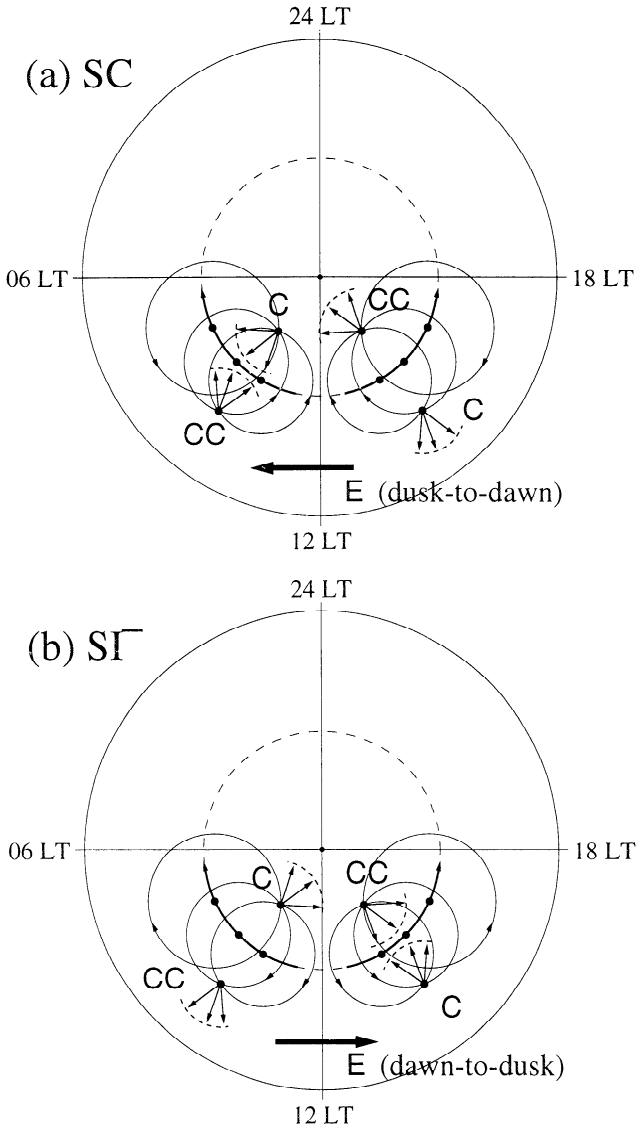

Figure 12. (a) A model for the polarization of SC. C and CC represent clockwise and counterclockwise polarization, respectively. The rotational sense becomes opposite at each side of the locus of the center of a current vortex moving in the polar ionosphere. Figure 12a is reproduced from *Nagano et al.* [1985]. (b) An applied model for the polarization of SI⁻ obtained by reversing the current direction in Figure 12a.

To explain the latitudinal reversal of the sense of SC polarization, *Nagano et al.* [1985] suggested another model shown in Figure 12a. When a compressional wave propagates toward the Earth in the dayside magnetosphere, a dusk-to-dawn electric field along the wavefront is transmitted along the lines of force to the northern polar ionosphere and produces twin-vortex-type ionospheric currents. As the interplanetary shock sweeps past the magnetosphere, the two vortices move from noon toward the dawnside and duskside. As a result, the magnetic field produced by the current vortices changes its direction at a fixed point on the ground. In the morningside the rotational sense of the

horizontal magnetic vector is counterclockwise (CC) in the lower-latitude side of the locus of the center of the vortex and clockwise (C) in the higher-latitude side. In the afternoonside the rotational sense is clockwise (C) in the lower-latitude side and counterclockwise (CC) in the higher-latitude side.

We should contemplate whether or not this model is applicable to the case of SI^-. In the case of SI^- a dawn-to-dusk electric field along the rarefaction wavefront is transmitted to the northern polar ionosphere. Figure 12b is a model applied to SI^- which is obtained by reversing the current direction in Figure 12a. Similarly, the longitudinal movement of two current vortices produces the field rotation. It is found that the rotational sense of the horizontal magnetic vector at a fixed point on the ground is the same as that of SC. Therefore the model can be applied to SI^-. We suggest that the contribution from this mechanism is dominant in producing the polarization of SC and SI^- and that the polarization is sometimes modified by Psc and/or particle precipitation. Direct observations of the longitudinal movement of the twin-vortex current pattern during PI are desired.

The magnetic latitude where the polarization reversal occurs is consistent with the center of the current vortex described in Figure 8, which also confirms the model in Figure 12. The reversal occurred around 80° MLAT, somewhat higher than the reversal associated with SCs which was found to occur between 64° and 72° [*Araki and Allen,* 1982]. The difference between compression and expansion of the magnetosphere could possibly explain the latitude change. Examination of a larger number of SI^- events could help to provide an answer.

The longitudinal reversal of the sense of polarization occurred at around 1200 LT. *Wilson and Sugiura* [1961] reported that the longitudinal boundary line was located at 1000 LT in the dayside hemisphere. It may depend on the angle at which shocks or discontinuities collide with the magnetosphere if the model shown in Figure 12 is valid.

If an interplanetary shock or discontinuity is inclined toward dawn or dusk, compression (rarefaction) of the magnetosphere would start at a point away from the subsolar point. The compression (rarefaction) wavefront therefore propagates in the magnetosphere asymmetrically with respect to the noon-midnight meridian. After the passage of the wavefront to the magnetotail, the dayside magnetosphere will have been in a symmetrically compressed (expanded) state owing to the enhanced (reduced) dynamic pressure behind the shock or discontinuity. Therefore the effect of inclination is detectable only during the early part of the geomagnetic disturbance. We have suggested two candidates that represent the "inclination effect": (1) the temporal variation of the direction normal to the compression/rarefaction wavefront in the magnetosphere and (2) the longitudinal boundary at which the rotational sense of the SI polarization reverses. Another possible candidate is the distribution of SI onset times at low-latitude stations, which might suggest how the compressional HM wave propagates to the ionosphere. However, it is usually difficult to detect the precise onset time because the shielding current flowing in the ionosphere suppresses the sudden increase/decrease in the H component on the ground to make a slow rise/fall of SI. A large and steep pulse and high time resolution geomagnetic observations are necessary for the detailed analysis of the onset time and the propagation of the disturbances.

5. Conclusion

1. Geomagnetic variations of SI^- observed on the ground are well explained by the model for SC by reversing the direction of the electric current used in the model.

2. The nominal peak time of the preliminary positive impulse has a fairly clear dependence on the geomagnetic latitude, which can be explained by a superposition of the DL and DP field that are dominant at low- and high-latitude, respectively. This tendency is not limited to the SI^-. The PRI at the time of SC would have the same feature.

3. The distribution of polarization sense of SI^- shows similar dependence on local time and latitude as that of SC. Thus SI^- is not merely a mirror image of SC in the polarization. The polarization distribution of both SC and SI^- can be explained by the longitudinal movement of ionospheric current vortices from dayside to nightside. There is an inherent field rotation during PI of SC and SI^- even if no pulsations exist.

4. To examine the transition of the direction normal to the SI wavefront in the magnetosphere and to examine the longitudinal reversal of the polarization sense would be helpful for determining the collision angle between the magnetosphere and the interplanetary shock or discontinuity.

Acknowledgments. MAGIC data acquisition on the Greenland ice cap (sites MCN, MCW, MCE) is supported by NSF through a grant to SPRL, University of Michigan. MAGIC data used in this study were kindly provided by the PI, C. R. Clauer. We express our sincere thanks to all the members of the geomagnetic field observation network teams: the Greenland chain, the IMAGE chain, the SAMNET chain, and 210° MM chain. We gratefully acknowledge K. W. Ogilvie for use of the Wind plasma data and R. P. Lepping for use of the Wind magnetometer data. We thank D. Wilkinson for providing the GOES 7 magnetic field data and T. Goka and H. Matsumoto at NASDA for providing ETS VI MAM data. The author also thanks T. Iyemori at DACGSM, Kyoto University, for his assistance in analyzing the geomagnetic field data and both referees for their suggestions for improving the paper. Parts of the geomagnetic data used in the present study were obtained from the World Data Center for Geomagnetism, Kyoto University.

Hiroshi Matsumoto thanks P. Chi and G. Rostoker for their assistance in evaluating this paper.

References

Araki, T., Global structure of geomagnetic sudden commencements, *Planet. Space Sci., 25,* 373, 1977.

Araki, T., A physical model of geomagnetic sudden commencement, in *Solar Wind Sources of Magnetospheric Ultra-Low-Frequency Waves, Geophys. Monogr. Ser.,* vol. 81, edited by M. J. Engebretson, K. Takahashi, and M. Scholer, pp. 183, AGU, Washington, D. C., 1994.

Araki, T., and J. H. Allen, Latitudinal reversal of polarization of the geomagnetic sudden commencement, *J. Geophys. Res., 87,* 5207, 1982.

Araki, T., and H. Nagano, Geomagnetic response to sudden expansions of the magnetosphere, *J. Geophys. Res., 93,* 3983, 1988.

Araki, T., T. Iyemori, and T. Kamei, Sudden commencements observed by MAGSAT above the ionosphere, *J. Geomagn. Geoelectr., 36,* 507, 1984.

Araki, T., J. H. Allen, and Y. Araki, Extension of a polar ionospheric current to the nightside equator, *Planet. Space Sci., 33,* 11, 1985.

Kokubun, S., Characteristics of storm sudden commencement at geostationary orbit, *J. Geophys. Res., 88,* 10,025, 1983.

Nagai, T., T. Ondoh, H. Matsumoto, T. Goka, T. Fukuda, M. Nose, T. Iyemori, K. Takahashi, and S. Kokubun, ETS-VI magnetic field observations of the near-earth magnetotail during substorms, *J. Geomagn. Geoelectr., 48,* 741, 1996.

Nagano, H., and T. Araki, Seasonal variation of amplitude of geomagnetic sudden commencements near midnight at geostationary orbit, *Planet. Space Sci., 34,* 205, 1986.

Nagano, H., T. Araki, H. Fukunishi, and N. Sato, Characteristics of polarization of geomagnetic sudden commencements at geostationary orbit, *Mem. Natl. Inst. Polar Res. Spec. Issue Jpn., 36,* 123, 1985.

Nagata, T., and S. Abe, Notes on the distribution of SC* in high latitudes, *Rep. Ionos. Space Res. Jpn., 9,* 33, 1955.

Saito, T., and S. Matsushita, Geomagnetic pulsations associated with sudden commencements and sudden impulses, *Planet. Space Sci., 15,* 573, 1967.

Samson, J. C., J. A. Jacobs, and G. Rostoker, Latitude dependent characteristics of long-period geomagnetic micropulsations, *J. Geophys. Res., 76,* 3675, 1971.

Takeuchi, T., T. Araki, R. P. Lepping, T. Yamamoto, S. Kokubun, T. Nagai, and T. Iyemori, A magnetic cloud with unusual structure and corresponding bow shock movement observed on May 13, 1995, *Geophys. Res. Lett., 25,* 3269, 1998.

Tamao, T., The structure of three-dimensional hydromagnetic waves in a uniform cold plasma, *J. Geomagn. Geoelectr., 16,* 89, 1964.

Tsyganenko, N. A., and D. P. Stern, Modeling the global magnetic field of the large-scale Birkeland current systems, *J. Geophys. Res., 101,* 27,187, 1996.

Wilson, C. R., and M. Sugiura, Hydromagnetic interpretation of sudden commencement of magnetic storms, *J. Geophys. Res., 66,* 4097, 1961.

Yumoto, K., and the 210 (deg) MM Magnetic Observation Group, The STEP 210 (deg) magnetic meridian network project, *J. Geomagn. Geoelectr., 48,* 1297, 1996.

T. Araki and T. Takeuchi, Department of Earth and Planetary Science, Graduate School of Science, Kyoto University, Kyoto 606-8502, Japan. (tomtakc@kugi.kyoto-u.ac.jp)

H. Luehr, GeoForschungs Zentrum, Telegrafenberg, D-14473 Potsdam, Germany.

I. R. Mann and D. K. Milling, Department of Physics, University of York, York YO10 5DD, England, U.K.

T. Nagai, Department of Earth and Planetary Sciences, Tokyo Institute of Technology, Ookayama, Tokyo 152-8551, Japan.

O. Rasmussen and J. Watermann, Solar-Terrestrial Physics Div., Danish Meteorological Institute, Lyngbyvej 100, DK 2100 Copenhagen, Denmark.

K. Shiokawa, Solar-Terrestrial Environmental Laboratory, Nagoya University, Toyokawa, Aichi 442-0061, Japan.

K. Yumoto, Department of Earth and Planetary Sciences, Kyushu University, Fukuoka 812-8581, Japan.

(Received November 10, 1999; revised February 8, 2000; accepted March 22, 2000.)